

Development and performance evaluation of intelligent algorithm for optimal control of a hybrid heat pump system during the cooling season

Yong Gi Jung^a, Kwang Ho Lee^b, Bo Rang Park^a, Tae Won Kim^a, Jin Woo Moon^{a,*}

^a School of Architecture and Building Science, Chung-Ang University, 84, Heukseok-ro, Dongjak-gu, Seoul 06974, Republic of Korea

^b Department of Architecture, College of Engineering, Korea University, 145, Anam-ro, Seongbuk-gu, Seoul 02841, Republic of Korea

ARTICLE INFO

Keywords:

Hybrid Heat Pump System
Artificial Neural Network
Intelligent Optimal Control
Heat Storage Tank
Indoor

ABSTRACT

The purpose of this study is to develop a control method for a hybrid heat pump system based on an artificial neural network (ANN) to reduce energy use and create a more comfortable thermal environment. The proposed optimal control method uses an ANN-based predictive model to predict the heat storage tank and indoor temperature during the cooling period and controls the flow rate of the circulation pump on the heat source and load side of the system. The performance of the predictive model for the heat storage tank temperature ($R^2 = 0.9988$; coefficient of variation of the root mean square error [CV(RMSE)] = 1.06 %; normalized mean bias error [NMBE] = 0.16 %; and mean absolute error [MAE] = 0.09°C) and the indoor temperature ($R^2 = 0.9893$; CV (RMSE) = 1.66 %; NMBE = 0.16 %; and MAE = 0.15°C) was excellent. The temperature control of the heat storage tank using the optimal algorithm exhibited an improvement of 18.39 % for the CV(RMSE), 3.10 % for the NMBE, and 1.31 °C for MAE compared with rule-based. For the indoor temperature, the optimal algorithm improved the CV(RMSE) by 1.30 %, NMBE by 0.42 %, and MAE by 0.29°C compared to rule-based. The energy use was reduced by 52.85 % for the entire system using the optimal control method compared with the existing control strategy under similar outdoor conditions. Using the proposed control method, it is thus possible to improve thermal comfort and reduce carbon emissions in the building sector by improving the control and energy performance of hybrid heat pump systems.

1. Introduction

According to the International Energy Agency (IEA), annual greenhouse gas emissions from energy consumption have increased steadily [1,2]. These emissions result in a variety of adverse outcomes, including climate change, acid rain, an increase in respiratory and cardiovascular diseases, and the proliferation of infectious diseases [3,4]. To address these social and environmental concerns, countries worldwide have established a variety of policies, such as setting carbon neutrality targets for 2050 and introducing measures to reduce greenhouse gas emissions and achieve carbon neutrality [5]. In particular, there has been a drive toward greater energy conservation in the construction sector, which is responsible for 40 % of total carbon emissions [6]. Building heating and cooling, which accounts for 54 % of the energy used in the building sector, has become particularly significant in this regard given the greater energy usage due to the rising demand for improved thermal comfort during abnormal climate events [7,8].

To reduce energy consumption in building heating and cooling systems, numerous technologies are currently under development, including high-efficiency heat pump systems and renewable energy technologies [9–11]. However, the efficiency of heat pumps differs greatly depending on the outdoor temperature due to the heat exchange process [12]. In the case of renewable energy, since solar heat, solar energy, and geothermal energy are used as a single heat source, there are limitations such as unstable energy supply and demand due to weather conditions and performance degradation that occurs when continuous geothermal use is used [13].

To overcome these disadvantages, multi-source hybrid heat pump systems have attracted recent attention [14,15]. A hybrid heat pump system combines a heat pump with additional heat sources, such as heat storage or multiple renewable energy sources, as well as a boiler [16,17]. Hybrid heat pump systems can reduce energy usage in buildings due to the higher energy efficiency arising from the installation of additional equipment such as heat storage tank, renewable energy

* Corresponding author.

E-mail addresses: popopop12@cau.ac.kr (Y.G. Jung), kwhlee@korea.ac.kr (K.H. Lee), pbrighten@cau.ac.kr (B.R. Park), xngilsh@cau.ac.kr (T.W. Kim), gilbert73@cau.ac.kr (J.W. Moon).

<https://doi.org/10.1016/j.enbuild.2024.113934>

Received 28 October 2023; Received in revised form 14 January 2024; Accepted 18 January 2024

Available online 22 January 2024

0378-7788/© 2024 Elsevier B.V. All rights reserved.

system [18,19]. In previous research, hybrid heat pump systems with various heat sources have been studied, confirming the potential for significant energy savings [20–22]. However, because hybrid heat pump systems generally have a complicated configuration due to the combination of various elements, system design can incur significant time and monetary costs, while system-integrated control can be difficult [23]. Most system control methods are rule-based based on temperature [24,25]. Rule-based control involves the individual control of equipment components based on specific temperature thresholds, meaning it is unable to adapt to real-time load variation due to building characteristics, local conditions, and seasonal changes, thus reducing operational efficiency and wasting stored thermal resources [26].

As a result, empirical control methods that require expert knowledge or proportional-integral-derivative (PID) control have been developed [27,28]. PID control reduces variation in performance by feeding the error between the output and input values back into the control system. However, control errors can still occur due to disturbances, and tuning is necessary when the building, operating, or outdoor air conditions change. Tuning also requires the experience and knowledge of a professional and, even if automatic tuning is employed, non-linear systems cannot be tuned using a general linear method. A hybrid heat pump system combines various components, and the operating conditions for each of these components are different, meaning that the system operating conditions are non-linear [29]. Consequently, conventional control methods such as rule-based and PID control face limitations in terms of achieving integrated control for hybrid heat pump systems.

Artificial neural networks (ANNs) can be used to resolve the limitations associated with existing control systems. In particular, ANNs can model non-linear input–output relationships between the components of hybrid heat pump systems, thus enabling integrated control [30,31], and can adapt to environmental changes via real-time retraining, reducing the time and financial costs associated with system design [32]. In hybrid heat pump systems that use a PVT system as a renewable heat source combined with a heat storage tank (HST), the hot water produced by the PVT heat pump can be used during the heating period but not the cooling period. Because the heat source and load sides of the system are individually controlled based on the temperature via the HST, integrated control measures are essential. In addition, even if the performance of the heat storage tank and heat pump is improved, the overall coefficient of performance for the system decreases because the circulation pumps within the system operate individually, thus an integrated control method is needed to improve energy efficiency.

Recently, numerous studies have been conducted to predict the performance of hybrid heat pump systems, develop predictive models, and establish optimal control strategies for these systems. Wang et al. [33] studied the performance of a hybrid heat pump system that combined solar energy and geothermal energy, demonstrating the possibility of reducing energy consumption. In addition, Gang et al. [34] developed a geothermal exchanger predictive model for a hybrid geothermal heat pump system and predicted the water exiting the ground heat exchanger outlet temperature. Sichilalu et al. [35] conducted research on the optimal control of a hybrid heat pump system that combined fuel cells, wind power, and solar energy, confirming the potential for cost savings resulting from enhanced energy performance. However, previous research has been limited to the development of predictive models for single heat sources, which have been tested using simulations. As such, there has been a lack of actual control studies and a lack of research on the integrated control of hybrid heat pump systems.

Therefore, the purpose of the present study was to propose an integrated control method to improve cooling-period control and the energy performance of a hybrid heat pump system. To achieve this, an intelligent optimal control algorithm based on an ANN was developed, with the aim to improve control performance and reduce energy consumption. The predictive model included in the optimal control algorithm predicted the HST and room temperature after 10 min and was used to select the optimal circulation pump flow rate on the heat source and load

sides. The performance of the control algorithm was evaluated by conducting an empirical experiment using a field system.

2. Overview of the control algorithm and predictive model development

This study was conducted in four phases (Fig. 1). First, a database was established to train the predictive model. The data was obtained from TRNSYS 18 simulations and consisted of HST and indoor temperature data every 10 min according to changes in the flow rate of the circulation pump on the heat source and load sides of the hybrid heat pump system. Second, the optimal control algorithm, which controls the system based on an ANN, was developed and compared with a conventional rule-based algorithm that turns on/off depending on the temperature. Third, predictive models for the HST and indoor temperature were developed using the training data. The performance of the developed predictive models was assessed using evaluation metrics such as R^2 , the coefficient of variation of the root mean square error (CV (RMSE)), normalized mean bias error (NMBE), and mean absolute error (MAE). Finally, the developed optimal control algorithm was embedded in a field system to evaluate its performance in terms of overall control and energy consumption. Control performance was assessed using the CV(RMSE), NMBE, and MAE metrics, while energy performance was analyzed using energy consumption data for the overall system, heat pump, circulation pumps, and fan coil units (FCUs).

2.1. Building and system overview

The building and hybrid heat pump system used in this study were located in Busan, Korea (Table 1). The average temperature in Busan during August, the warmest month of the cooling period, is 26.1°C and the average humidity is 78.5 %, making it a warm and humid climate (Cfa) according to the Köppen climate classification. The building had a floor area of 110.16 m², and the exterior U-value was 0.32 W/m²K for the exterior wall, 0.35 W/m²K for the floor, 0.18 W/m²K for the roof, and 1.51 W/m²K for the windows. The solar heat gain coefficient (SHGC) of the window was 0.37 W/m²K.

The dual heat source system combined a PVT heat pump and an air source heat pump in parallel. The heat was stored in the HST in accordance with the period (i.e., cooling or heating), and the stored heat was supplied to the FCU to cool or heat the room. Hot water was stored using the PVT and Auxiliary components, and the HST during the heating period was stored using the PVT and air source heat pumps. During the cooling period, the HST was cooled using the air source heat pump. The

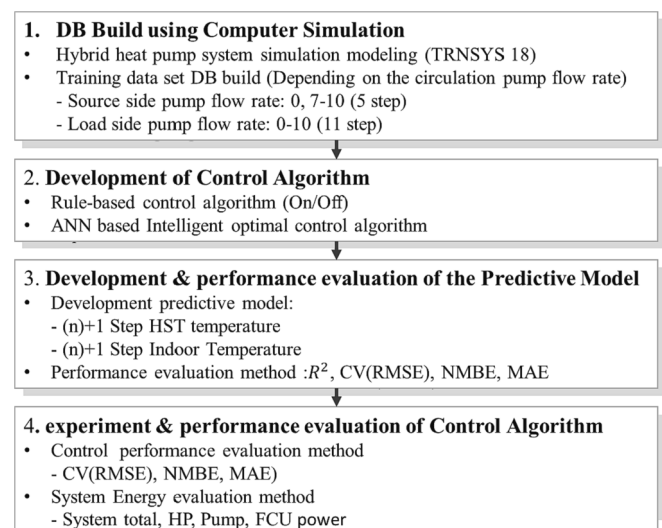
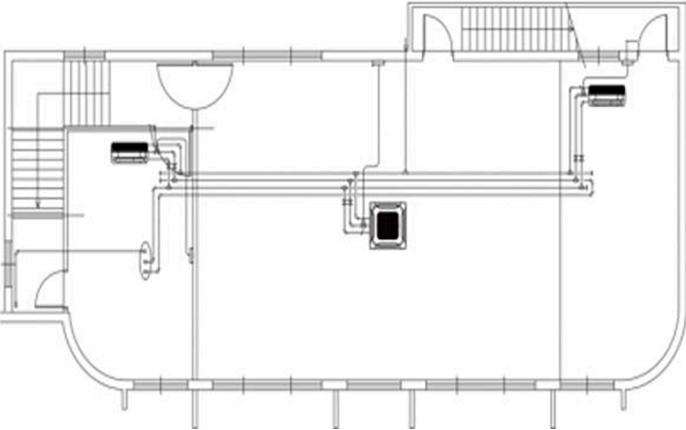



Fig. 1. Overview of the research process for the present study.

Table 1
Experiment building and system overview.

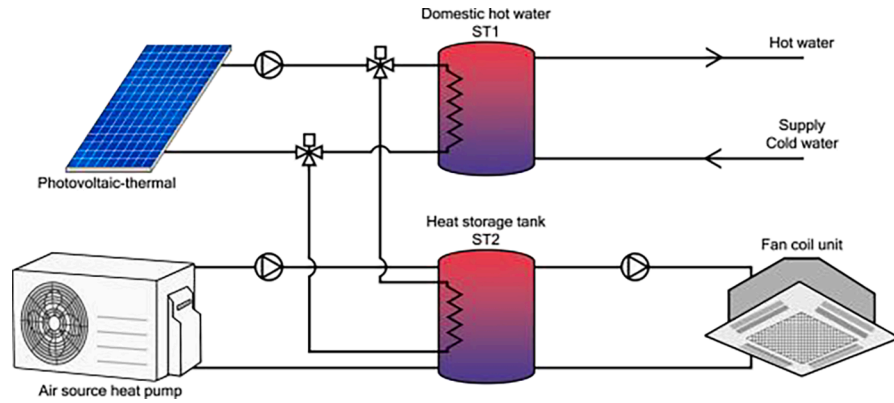
Building overview	
	
<p>Region Climate zone Floor area U-Value</p> <p>External wall Floor Roof Window</p> <p>SHGC Window</p> <p>system overview</p>	<p>Gi-jang, Buans, Korea Köppen – Cfa, 4A 110.16m² 0.32 W/m²·K 0.35 W/m²·K 0.18 W/m²·K 1.51 W/m²·K 0.37 W/m²·K</p>

3

(continued on next page)

Table 1 (continued)

Building overview



4

PVT area			1.012 m × 19.72 m
Heat pump	capacity	Heating	9 kW
		Cooling	8 kW
FCU	Power		2.4 kW
	capacity	Heating	21.49 kW(9.82 kW + 11.67 kW)
		Cooling	15.88 kW(8.47 kW + 7.41 kW)
			0.21 kW(0.09 kW + 0.12 kW)
Circulation pump	Power		26°C
	Setpoint		±1°C
	Deadband	Source	43.15LPM-50.80LPM / 4 step
	Flowrate	Load	10.22LPM-36.55LPM / 10 step
Heat Storage tank	Power	Source	0.18 kW-0.24 kW
	capacity	Load	0.12 kW-0.24 kW
	Setpoint		300L
Cooling Period	Deadband		10°C
			±2°C
Occupancy Time			May, June, July, August, September 09:00–18:00

PVT was installed at 1.012 m × 19.72 m. heat pump had a heating capacity of 9 kW, a cooling capacity of 8 kW, and a power consumption of 2.4 kW. The capacity of the HST was 300 L, which was installed indoors to minimize the influence of solar radiation. The FCU consisted of two 1-way units and one 4-way unit, totaling heating capacity 21.49 kW (9.82 kW + 11.67 k), cooling capacity 15.88 kW (8.47 kW + 7.41 kW), while the FCU fan power consumption was 0.21 kW (0.09 kW + 0.12 kW). For the circulation pump, the heat pump side was 50.80 LPM with a power consumption of 0.19 kW, while the FCU side was 36.55 LPM with a power consumption of 0.15 kW. The cooling period was set from May to September with an HST temperature of 10°C and an indoor temperature of 26°C, and the building occupancy period was set to 09:00–18:00 [36].

The flow rate of the circulation pump was controlled between levels 0 and 10 in 1-step increments (off = 0). When turned on, the heat source side had a flow rate of 7–10, which is the minimum required flow rate for the heat pump system, while the load side had a potential flow rate of 1–10. The system was monitored and controlled in real-time using a WEP-based cloud platform linked to Internet of Things devices, with sensing data stored in an SQL database every minute. The system was controlled using the MQTT protocol.

2.2. Control algorithms

2.2.1. On/off rule-based control

The rule-based algorithm turned the system on/off within a deadband range to satisfy the setpoints (Fig. 2). The operating conditions for this algorithm are presented in Table 2.

Step A was a data acquisition step in which time and sensor data were acquired, with the operating status determined according to the time and day of the week. The PVT inlet/outlet water temperature, heat pump inlet/outlet water temperature, heat source and load side HST inlet/outlet temperature, FCU inlet/outlet water temperature, indoor/outdoor temperature, circulation pump flow rate and heat pump and FCU power consumption were obtained for system control.

Step B involved PVT-side operation control for the storage of heat in the HST, which was turned on/off within the deadband range of the setpoint. The hot water storage system stored heat when the lower limit of the deadband was reached, stopping only when the upper limit of the deadband was reached. In the present study, the setpoint was 60°C and the deadband was 2°C, thus the system turned on when the HST

temperature was lower than 58°C and turned off when it exceeded 62°C. The HST first stored hot water using the PVT heat source when heat storage was possible because the PVT outlet temperature was higher than the lower limit of the deadband. In cases where PVT heat storage was not possible, the hot water was stored using the AUX heat source.

Step C was the HST heat storage stage, which was turned on/off within the deadband range of the setpoint. When the upper limit of the deadband was reached, the system operated in cooling mode, and when the lower limit was reached, operation was halted. Here, the setpoint was 10°C and the deadband was 2°C, thus if the temperature of the HST was higher than 12°C, the heat pump and circulation pump were operated to cool the HST. When the temperature dropped below 8 °C, the system turned off. The circulation pump operated at 10 (50.80 LPM) when turned on and at 0 (0 LPM) when turned off.

Step D was the indoor cooling phase. When the indoor temperature exceeded the deadband lower limit of the indoor setpoint, the system started indoor cooling mode, ending when the indoor temperature reached the deadband upper limit. The indoor setpoint was 26°C and the deadband was 1°C, thus, when the indoor temperature exceeded 27°C, the FCU and circulation pump turned on for indoor cooling. When the room temperature was lower than 25°C, the system stopped. The circulation pump operated at 10 (36.55 LPM) when turned on and at 0 (0 LPM) when turned off. Finally, Step E controlled the system using the transmission of system control signals.

2.2.2. Intelligent optimal control algorithm

Using the rule-based algorithm, the system was continuously turned on and off within the deadband range to satisfy the setpoints, with the circulation pump flow rate operating between 0 % and 100 %. This approach had the disadvantage of being unable to adapt to partial loads, while the heat pump operated continuously. And if the goal is only to improve the control accuracy, it is possible to move closer to the setpoint by narrowing the deadband range of the existing rule-based algorithm, but this may waste energy during operation because the system is continuously turned on and off. In addition, under existing control methods, if building or weather conditions change, manual intervention is required to maintain control. On the other hand, with artificial neural network-based optimal control algorithms, the system can be optimally controlled in response to partial loads and can automatically adapt by retraining the prediction model when conditions change. To address

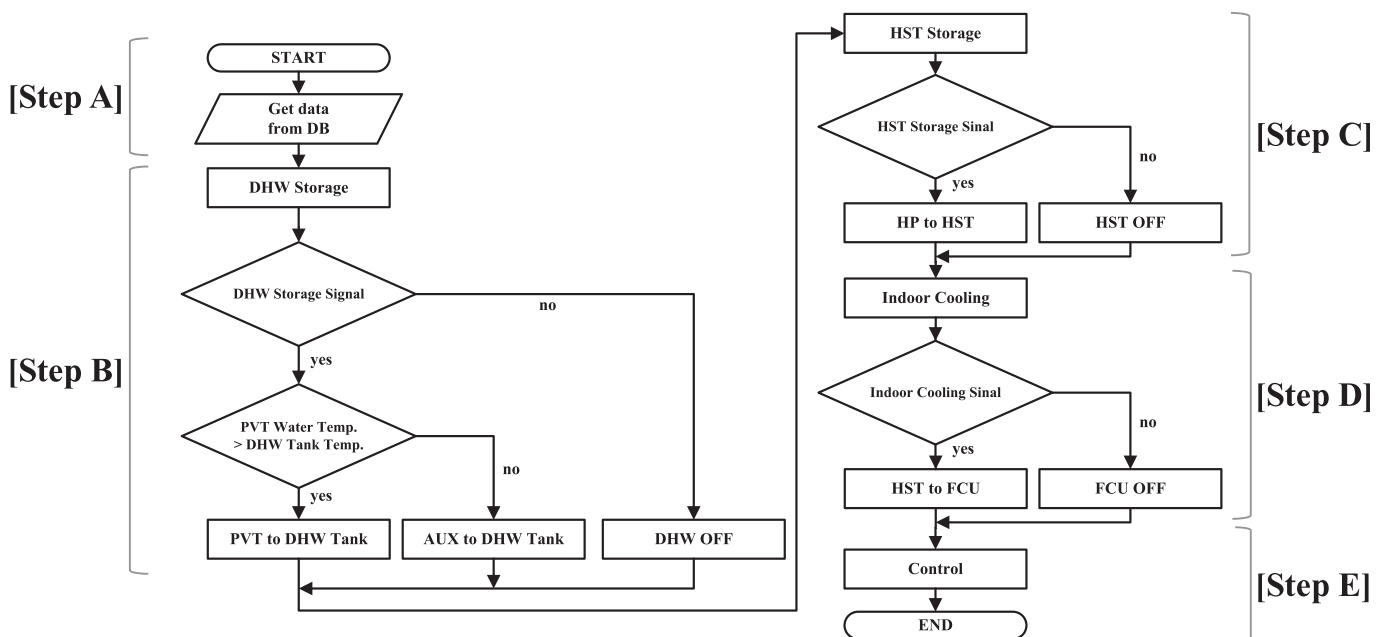
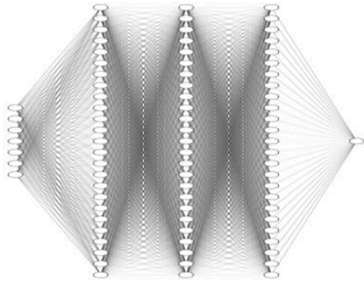
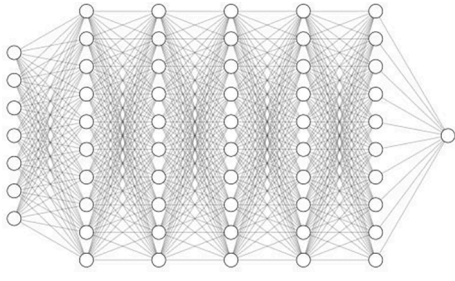


Fig. 2. Rule-based control algorithm flow chart.

Table 2
Details of the predictive models for the HST and indoor temperature.

	HST	Indoor
Input layer	<ul style="list-style-type: none"> Indoor temperature (n) [°C] Outdoor temperature (n) [°C] HST temperature (n) [°C] HP water inlet and outlet temperature (n) [°C] Pumps 1 and 2 circulating water flow rate (n) [kg/h] 	<ul style="list-style-type: none"> Indoor temperature (n) [°C] Outdoor temperature (n) [°C] FCU water inlet and outlet temperature (n) [°C] Pump 2 circulating water flow rate (n) [kg/h]
Hidden layers	25–25–25	13–13–13–13
Output layer	<ul style="list-style-type: none"> HST temperature (n + 1) [°C] 	<ul style="list-style-type: none"> Indoor temperature (n + 1) [°C]
Diagram		
	Input [7]/Hidden [25–25–25]/Output [1]	Input [5]/Hidden [13–13–13–13]/Output [1]

these limitations and simultaneously enhance control performance, energy efficiency, and adaptability, an ANN-based intelligent optimal control algorithm was developed (Fig. 3).

Step A was the same as for the rule-based algorithm. in which time

and sensor data was acquired, with the operating status determined according to the time and day of the week. The PVT inlet/outlet water temperature, heat pump inlet/outlet water temperature, heat source and load side HST inlet/outlet temperature, FCU inlet/outlet water

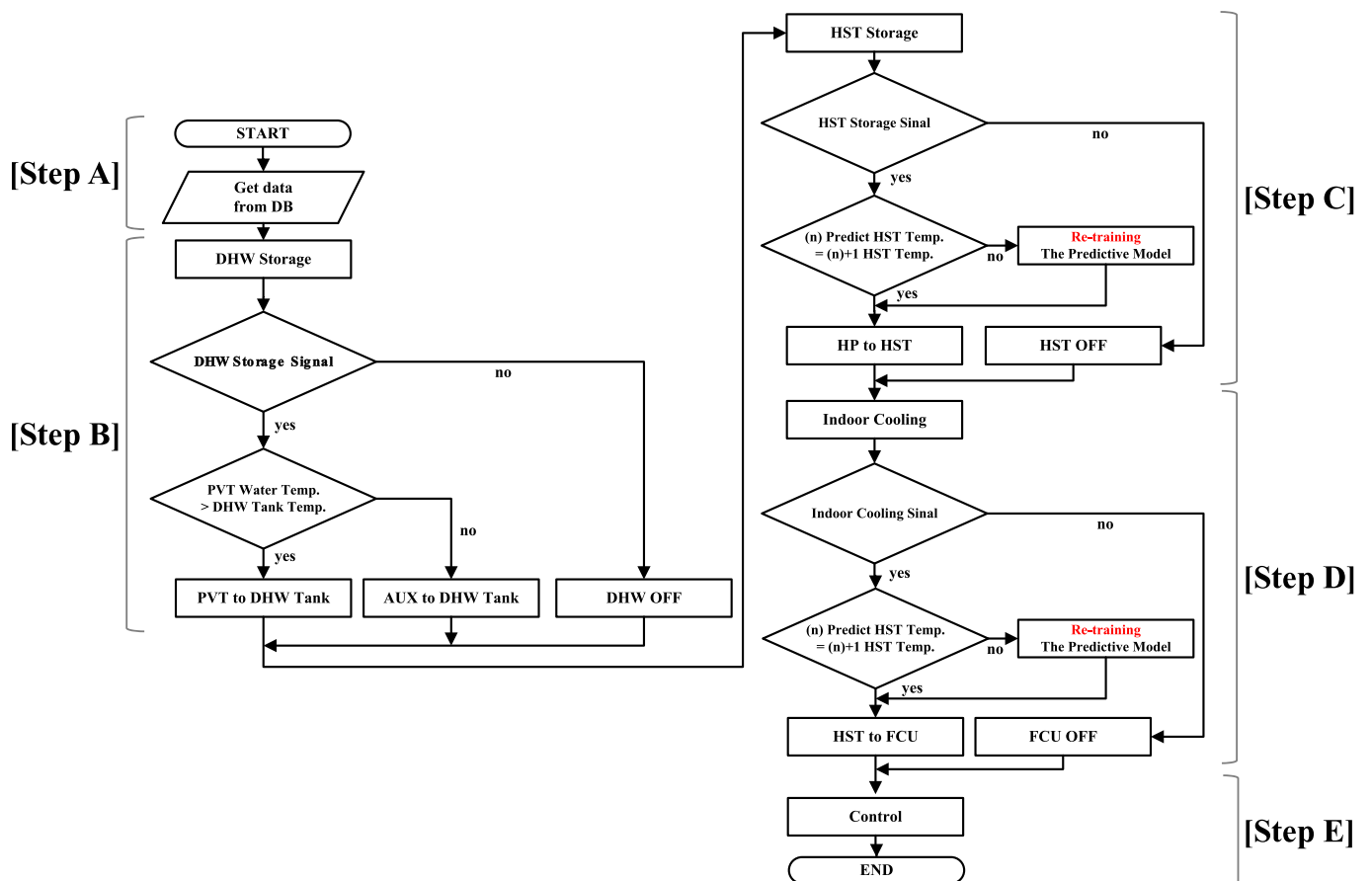


Fig. 3. Overview of the proposed optimal control algorithm.

temperature, indoor/outdoor temperature, circulation pump flow rate, and heat pump and FCU power consumption were obtained for system control.

Step B involved PVT-side control for heat storage in the HST, with the hot water storage turned on/off within the deadband range of the setpoint. The hot water storage system stored heat when the lower limit of the deadband was reached, and the system stopped when the upper limit of the deadband was reached. In the present study, the setpoint was 60°C and the deadband was 2°C, thus the system was operated when the HST temperature was lower than 58°C and turned off when it exceeded 62°C. The HST first stored hot water from the PVT heat source when heat storage was possible because the PVT outlet temperature was higher than the lower limit of the deadband. In cases where PVT heat storage was not possible, the hot water was stored using the AUX heat source.

Step C was the HST cooling step, in which the developed predictive model for HST temperature was employed to determine the circulation pump flow rate on the heat source side. The optimal circulation pump flow rate was selected to satisfy the HST setpoint during the cooling period by predicting the HST temperature for step (n) + 1 at step (n). The circulation pump flow rate was controlled at levels 0, 7, 8, 9, and 10. If there was no error when comparing the value predicted at step (n) with the actual measurement at step (n) + 1, the process proceeded to the next step. If an error occurred, the data from step (n) was used to retrain the predictive model. When an error occurs between the step n + 1 heat storage tank temperature predicted by the prediction model at step n and the actual heat storage tank temperature at step n + 1, the prediction model is retrained by adding the data collected at step n to the training data input for the prediction model.

Step D was the indoor cooling stage, and a predictive model was employed to select the load-side circulation pump flow rate. The optimal circulation pump flow rate was selected to satisfy the indoor temperature setpoint during the cooling period by predicting the indoor temperature for step (n) + 1 at step (n). The circulation pump flow rate was controlled within the range of 0–10. If there was no error when comparing the value predicted at step (n) with the actual measurement at step (n) + 1, the process proceeded to the next step. If an error occurred, the data from step (n) was used to retrain the predictive model. Step E sent the pump flow rate selected by the algorithm to the system for optimal control. When an error occurs between the step n + 1 indoor temperature predicted by the prediction model at step n and the actual indoor temperature at step n + 1, the prediction model is retrained by adding the data collected at step n to the training data input for the prediction model.

2.3. Predictive model development

An ANN is a type of supervised learning algorithm designed to imitate the neural network structure of the human brain [37]. It consists of input, hidden, and output layers, with the output values determined based on the weights and biases between nodes in each layer. ANNs are capable of non-linear learning between input and output values, ensuring adaptability to changes in conditions, which is a limitation of existing hybrid heat pump systems [38–40]. Therefore, two predictive models based on the structure of an artificial neural network (ANN) were developed to learn the non-linear relationships between variables within the hybrid heat pump system. These models predicted the HST and indoor temperature 10 min ahead according to the circulation pump flow rate under the current conditions, with the circulation pump flow rate that came closest to the HST and indoor setpoint selected and employed in the control process.

The two developed predictive models are summarized in Table 2. Variables correlated with changes in temperature were selected as input using Eq. (1)–(2). The predictive model for the HST temperature used the step (n) heat pump inlet and outlet water temperature, the HST temperature, the indoor and outdoor temperature, the heat source, and the load-side circulation pump flow rate as input and then predicted the

step (n) + 1 HST temperature using three hidden layers (25–25–25).

The predictive model for the indoor temperature used the step (n) HST inlet and outlet water temperature, indoor and outdoor temperature, and load-side circulation pump flow rate as input and then predicted the indoor temperature at step (n) + 1 using four hidden layers (13–13–13–13).

$$Q_{source} = m_{fluid} * c_{fluid} * (T_{SS} - T_{SR}) \quad (1)$$

$$Q_{load} = m_{fluid} * c_{fluid} * (T_{LS} - T_{LR}) \quad (2)$$

where Q_{source} is the amount of circulating water for heat exchange on the heat source side (kcal/h), Q_{load} is the amount of circulating water for heat exchange on the load side (kcal/h), m_{fluid} and c_{fluid} are the specific heat at constant pressure and the circulating water flow rate, respectively (kcal/kg°C and kg/h), T_{SS} and T_{SR} are the heat-source-side HST circulating water inlet and outlet temperature (°C). T_{LS} and T_{LR} are the load-side FCU circulating water inlet and outlet temperature (°C)

Constructing a dataset based on experimental data is suitable for field system control, but acquiring the necessary data in this way can be limited because conditions such as the season and time of day constantly change. In addition, there may not be sufficient time to collect the appropriate data, and there is a possibility that the prediction model may be overfitted to the system. Therefore, simulations were used to construct the data based on changes to the circulation pump flow rate under the same conditions. Furthermore, even though data differences may have occurred, the learning data were derived from simulations because, by doing so, it was possible to evaluate the adaptability of the proposed approach through re-learning, which was one of the main goals of this study. Therefore, The training data for the predictive models was obtained using TRNSYS 18, with temperature data for the HST and indoor space collected 10 min ahead based on variation in the circulation pump flow rate (levels 0 and 7–10 on the heat source side and levels 0–10 on the load side).

In particular, the heat storage tank temperature prediction model used both the heat source-side and load-side circulation pump flow rates as input. This reflected the amount of heat used on the load side in the heat storage tank temperature prediction model when storing heat in the heat storage tank. If the flow rate for the circulation pump on the load side is high, the flow rate for the circulation pump on the heat source side must also increase due to the use of heat from the heat storage tank. Therefore, to reflect the use of heat on the load side in the selection of the flow rate for the circulation pump on the heat source side, both the heat source and the circulation pump flow rates on the load side were selected as input for the prediction model.

For the predictive models, the performance of ANN, SVM, and Tree ensemble was compared to select the ANN model with the best performance [41]. In addition, among the ANN structures, ANN with one hidden layer, DNN with multiple hidden layers, and RNN with recurrent neural network structure were evaluated for performance, and a DNN model-based predictive model was developed. The training dataset was divided into three subsets: 60 % for training, 20 % for validation, and 20 % for testing. In addition, to minimize the weight bias caused by differences in ranges between input variables, min–max normalization was employed to process the data so that the individual data points had a value between 0 and 1, as shown in Eq. (3). The predictive model hyperparameters were optimized using Bayesian optimization [42].

$$x'_i = \frac{x_i - \min(X)}{\max(X) - \min(X)} \quad (3)$$

where X is the input variable dataset, x'_i is the i -th value in the normalized dataset X , and x_i is the i -th datapoint in dataset X .

3. Performance evaluation of the predictive models and control algorithm

3.1. Performance of the predictive models

The performance evaluation of the predictive models was conducted using the R^2 , CV(RMSE), NMBE, and MAE to assess the relationship between the predicted values and actual measurements. An R^2 approaching 1 and an NMBE and a CV(RMSE) approaching 0 % represent stronger predictive performance. According to ASHRAE Guideline 14–2014, acceptable model performance is indicated by an R^2 greater than or equal to 0.8 and an NMBE and CV(RMSE) less than or equal to 10 % and 30 %, respectively [43]. The performance evaluation metrics were calculated using Eqs. (4)–(7):

$$R^2 = 1 - \frac{\sum_{i=1}^n (y_i - \hat{y}_i)^2}{\sum_{i=1}^n (y_i - \bar{y})^2} \quad (4)$$

$$CV(RMSE) = \frac{1}{\bar{y}} \sqrt{\frac{\sum_{i=1}^n (y_i - \hat{y}_i)^2}{n}} * 100(\%) \quad (5)$$

$$NMBE = \frac{1}{\bar{y}} \frac{\sum_{i=1}^n (y_i - \hat{y}_i)}{n} * 100(\%) \quad (6)$$

$$MAE = \frac{1}{n} \sum_{i=1}^n (|y_i - \hat{y}_i|) \quad (7)$$

where y_i is the actual value, \hat{y}_i is the predicted value, \bar{y} is the average of the actual value, and n is the number of observations.

The performance of the predictive models is displayed in Table 3. For the HST temperature, the R^2 was found to be more than 0.999, indicating a high correlation between the predictive and the actual measurements, while the CV(RMSE) was 1.06 % and the NMBE was 0.16 %, representing a predictive performance that exceeds ASHRAE recommended standards. The MAE was found to be 0.09 °C, confirming the excellent performance of the predictive model for HST temperature. For the indoor temperature, the R^2 was above 0.989, indicating a high correlation between the predictions and real measurements. The CV (RMSE) was 1.66 % and the NMBE was 0.16 %, which also met ASHRAE recommended standards. The MAE was 0.15 °C, verifying the excellent performance of the predictive model for indoor temperature.

3.2. Performance of the control algorithms

The control and energy performance of the optimal control algorithm was compared to that of the baseline rule-based control algorithm. The evaluation of the control performance focused on how closely the HST and indoor temperature followed their respective setpoint temperatures, as measured by the CV(RMSE), NMBE, and MAE. To assess the energy performance, the cumulative energy consumption of the system, instantaneous energy consumption, system operating time, and energy consumption relative to the daily average temperature were analyzed. The experiment was conducted from August to September 2022 for four days using rule-based control (08/29, 09/07, 09/19, 09/24) and four days based on the proposed optimal control method (09/05, 09/06, 09/22, 09/23).

Table 3
Predictive model performance for the HST and indoor temperature.

	HST Temperature	Indoor Temperature
R^2	0.9988	0.9893
CV(RMSE)	1.06 %	1.66 %
NMBE	0.16 %	0.16 %
MAE	0.09°C	0.15°C

3.2.1. Outdoor temperature during the experiment

The outdoor temperatures during the eight study days are presented in Fig. 4. During the four days of rule-based control, the maximum temperature was 34.10 °C, the minimum temperature was 15.40 °C, and the average temperature was 24.72 °C. For the four days of optimal control, the maximum temperature was 32.60 °C, the minimum temperature was 17.8 °C, and the average temperature was 25.61 °C. During the operating hours (09:00–18:00), rule-based control encountered a maximum temperature of 34.10 °C, a minimum temperature of 23.10 °C, and an average temperature of 28.64 °C. During optimal control, the maximum temperature during operating hours was 32.60°C, the minimum temperature was 22.20°C, and the average was 28.32°C.

3.2.2. Temperature control accuracy

The control performance of the developed control algorithm was evaluated based on the error between the actual temperature and the HST and room temperature setpoints using CV(RMSE), NMBE, and MAE. CV(RMSE) is an indicator of the error between the setpoint temperature and the actual controlled temperature, while the NMBE indicates the temperature control tendency compared to the setpoint temperature. When evaluating control performance, a negative (-) cooling period control error means excessive cooling compared to the setpoint, and a positive (+) control error means insufficient cooling. MAE is the average of the absolute value of the error.

The results for the HST temperature distribution are presented in Fig. 5. Under rule-based control, the four-day average CV(RMSE) was 31.35 %, the NMBE was -10.12 %, and the MAE was 2.24 °C. For the optimal control algorithm, the CV(RMSE) was 12.96 %, the NMBE was -7.02 %, and the MAE was 0.93°C, representing an improvement of 18.39 %, 3.10 %, and 1.31°C compared with rule-based control, respectively. Thus, the HST temperature was more evenly distributed and stable within the setpoint compared to rule-based control.

The indoor temperature distribution is presented in Fig. 6. Rule-based control produced a four-day average CV(RMSE) of 2.63 %, an NMBE of 0.82 %, and an MAE of 0.60 °C, compared to 1.33 %, -0.40 %, and 0.31 °C for the optimal control algorithm, representing an improvement of 1.30 %, 0.42 %, and 0.29 °C for the latter. When the optimal control algorithm was employed, the indoor temperature was as high as the HST. On 9/22, the outdoor temperature was lower than that on the other days, and it is believed that HST was stored in excessive cooling due to unstable MQTT communication. However, it was confirmed that the system reached a normal range during the 09:00–18:00 operating time. And, At 12:00 on September 23, the HST temperature dropped to approximately 5°C, which was believed to be due to overcooling of the system due to prediction errors in the forecast model. With existing rule-based algorithms, the system continues to operate until the next control step even if the heat storage tank temperature falls below the deadband lower limit. On the other hand, with optimal control, the entire period remained within the deadband range except for 12:00 on September 23. In addition, even though overcooling occurred due to a temperature prediction error in the heat storage tank, re-learning was conducted and the temperature returned to the setpoint range. Although it is difficult to ensure control accuracy due to the short re-learning period, it is believed that this can be improved through continuous re-learning. The overall control performance results are summarized in Table 4.

3.2.3. Energy reduction performance

As shown in Fig. 7, the energy usage during the system operating time (09:00–18:00) was compared for rule-based control and the optimal control algorithm. The energy consumption for the overall system, including the heat pump, circulation pump, and FCU, and the cumulative energy consumption of the heat pump, circulation pump, and FCU individually were analyzed. The energy consumption for each four-day period is presented in Table 5.

The total energy consumption was 33.24 kW for the rule-based

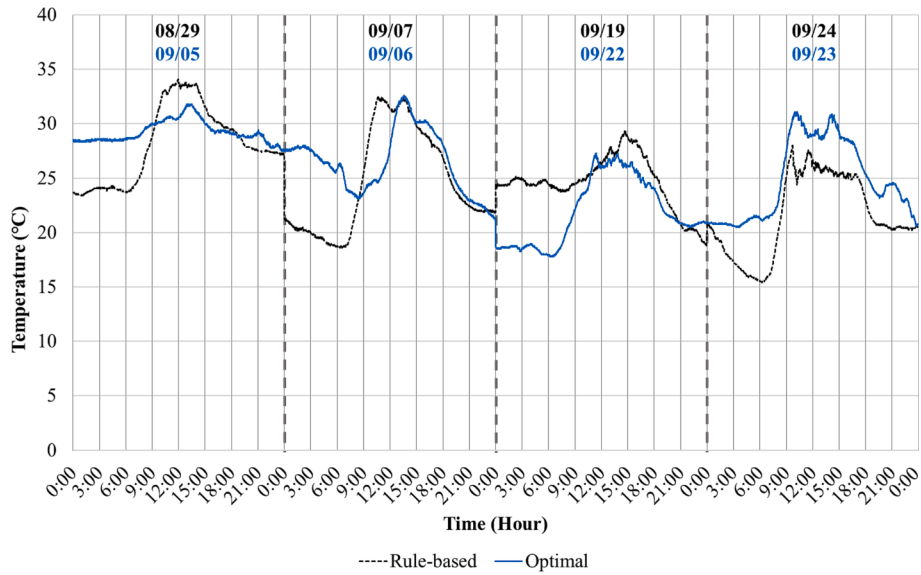


Fig. 4. Outdoor temperature during rule-based control (08/29, 09/07, 09/19, 09/24) and optimal control (09/05, 09/06, 09/22, 09/23).

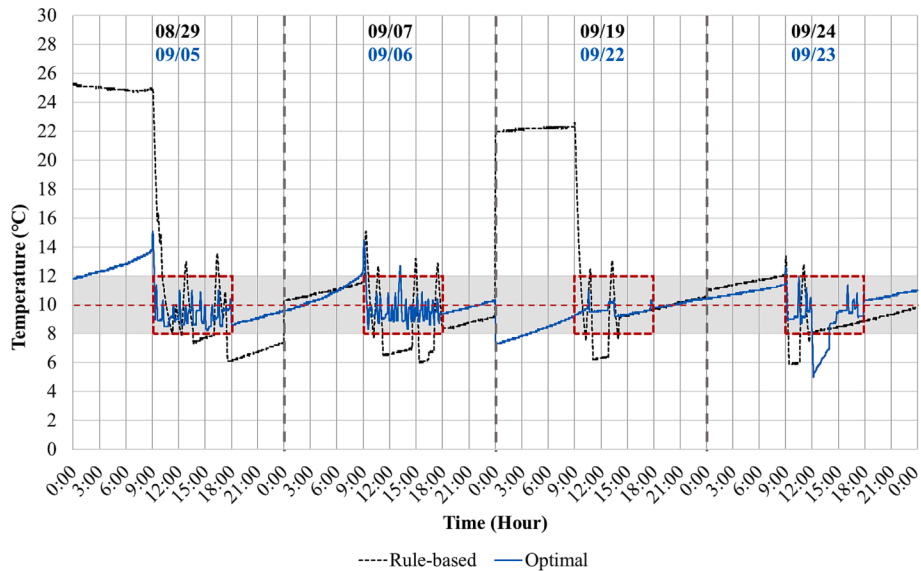


Fig. 5. HST temperature according to rule-based and optimal control (red line: setpoint [10°C]; gray box: deadband; red box: occupancy time [09:00–18:00]). (For interpretation of the references to colour in this figure legend, the reader is referred to the web version of this article.)

algorithm and 15.67 kW for the intelligent control algorithm. Under the rule-based algorithm, the heat pump consumed 22.91 kW, compared with 8.85 kW for the optimal control algorithm. The circulation pump consumed 8.41 and 7.86 kW under rule-based control and the optimal control algorithm, respectively, while the FCU consumed 1.82 and 2.80 kW, respectively. Thus, by employing the optimal control algorithm, total energy consumption was reduced by 17.57 kW (52.85 %), with individual reductions of 14.07 kW and 0.55 kW (61.39 % and 6.56 %) for the heat and circulation pumps, respectively, and an increase of 0.98 kW (53.82 %) for the FCU.

Under optimal control, the energy of the heat pump and circulation pump was reduced, but the energy consumption of the FCU increased. These results can be explained by the fact that, under rule-based control, when a load occurs, a section occurs where operation stops because the deadband is reached, while optimal control is conducted within the setpoint range. Thus, the system operates continuously to respond to the load under optimal control. For this reason, during the optimal control

experiment on September 22nd, the circulation pump and FCU energy consumption was higher than rule-based control because they operated continuously in response to the partial load. However, at the same time, the heat pump energy consumption, which accounted for the highest proportion of the total system energy use, was greatly reduced, resulting in a decrease in the overall system energy requirements.

Overall energy usage for the system was assessed according to the average outdoor temperature each day (Fig. 8). During optimal control, the slope of the trend line was lower than that of rule-based control, meaning that energy consumption was lower even at the same temperature. In particular, for cases [A-a] and [C-d], where the outdoor temperatures were similar, the proposed intelligent control resulted in lower energy consumption compared to rule-based control. However, in the case of [b-c], high energy consumption occurred at a relatively low temperature even with optimal control. This is believed to be because, although the average outside temperature was similar, the peak load for [b] was higher than that for [c], so system operation increased. On 08/

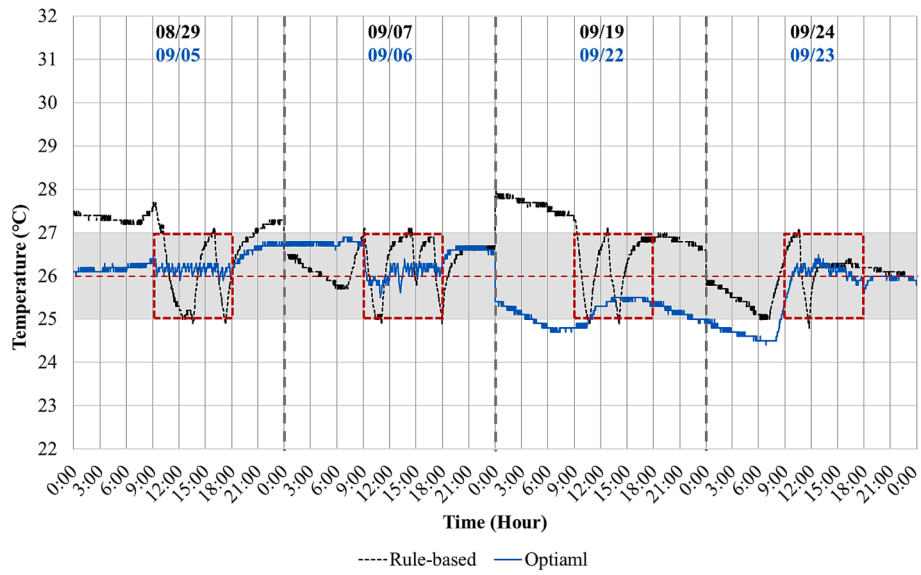


Fig. 6. Indoor temperature (red line: setpoint [26°C]; gray box: deadband; red box: occupancy time [09:00–18:00]). (For interpretation of the references to colour in this figure legend, the reader is referred to the web version of this article.)

Table 4

Control performance for the HST and indoor temperature using rule-based control and the optimal control algorithm.

Control	Date	HST temperature			Indoor temperature		
		CV(RMSE) [%]	NMBE [%]	MAE [°C]	CV(RMSE) [%]	NMBE [%]	MAE [°C]
Rule-based	08/29	35.58	1.54	2.49	3.17	0.22	0.72
	09/07	34.20	-18.39	2.74	2.80	1.12	0.67
	09/19	30.15	-4.69	1.93	2.69	1.02	0.63
	09/24	25.45	-18.95	1.91	1.87	0.90	0.40
	Aver.	31.35	-10.12	2.24	2.63	0.82	0.60
Optimal	09/05	12.71	-6.58	0.97	0.73	0.63	0.17
	09/06	11.24	-3.26	0.83	0.82	0.31	0.18
	09/22	5.55	-4.63	0.49	2.97	-2.80	0.71
	09/23	22.34	-13.60	1.44	0.82	0.28	0.17
	Aver.	12.96	-7.02	0.93	1.33	-0.40	0.31
Reduction		-18.39	-3.10	-1.31	-1.30	-0.42	-0.29

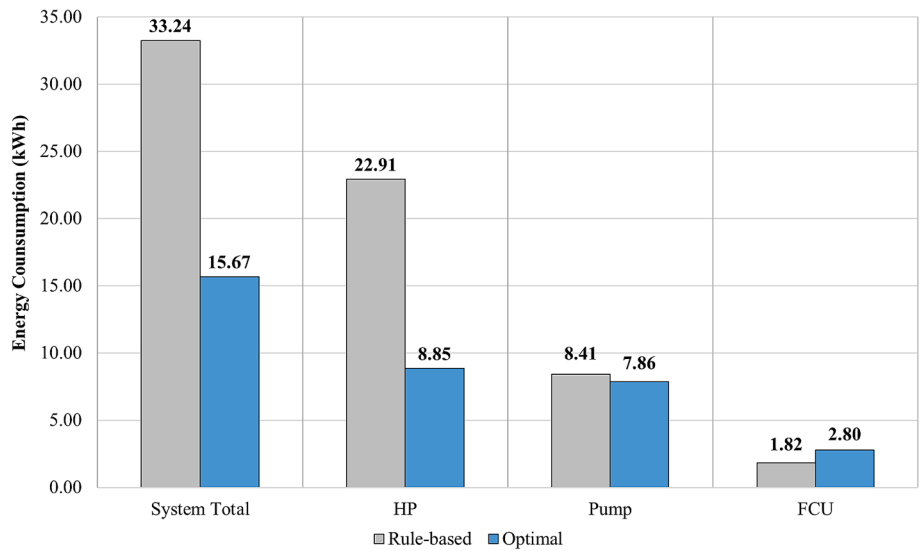


Fig. 7. Total energy consumption for rule-based and optimal control over four days.

Table 5
Daily energy consumption for rule-based and optimal control.

Control	Date	System [kW]	HP [kW]	Pump [kW]	FCU [kW]
Rule-based	08/29	14.975	10.849	3.32	0.783
	09/07	7.356	5.158	1.737	0.437
	09/19	3.303	1.983	1.075	0.219
	09/24	7.61	4.922	2.283	0.38
	Total	33.24	22.91	8.41	1.82
Optimal	09/05	4.183	2.701	1.191	0.267
	09/06	6.024	3.891	1.711	0.404
	09/22	4.174	1.886	4.174	2.018
	09/23	1.293	0.368	0.787	0.109
	Total	15.67	8.85	7.86	2.80
Reduction		-17.57 (52.85 %↓)	-14.07 (61.39 %↓)	-0.55 (6.56 %↓)	+0.98(+53.82 %↑)

29, the outside temperature was the highest recorded during the 8-day experiment schedule. The temperature was particularly high during the operating hours from 09:00 to 18:00, so the system operated continuously, resulting in high energy consumption. Though the energy consumption on day D was high, the energy consumption decreased under similar outdoor conditions (e.g., [A-a] and [C-d]), thus it is possible that energy consumption may decrease during optimal control under similar conditions to D.

The instantaneous power usage for the heat pump, circulation pump, and FCU during days with similar average outdoor temperatures in [C-d] (09/07, 09/05) and [A-a] (09/24, 09/22) is presented in Fig. 9. For [C-d], the heat pump was run for a total of 150 min under rule-based control and 110 min for optimal control. Additionally, for [A-a], rule-based control ran the heat pump for 63 min, compared with 42 min for optimal control. Thus, under rule-based control, instantaneous energy consumption was high, and the operating time was longer. On the other hand, under optimal control, the number of times the heat pump was switched on was high, but the instantaneous energy consumption was low, and the operating time was shorter, thus the cumulative energy

consumption was lower overall. This is because the heat pump starts and stops in response to partial loads due to the optimal control of the circulation pump flow rate when cooling the HST. Therefore, it was confirmed that energy-efficient operation can be achieved by preventing the excessive use of the heat pump.

For [C-d], the circulation pump operated for a total of 339 and 313 min under rule-based and optimal control, respectively. Additionally, under [A-a], the pump ran for a total of 238 min under rule-based control and 198 min for optimal control. Instantaneous energy consumption was high under rule-based flow because the flow rate was set at level 10, and the operating time was longer. In contrast, under optimal control, the number of times the pump was switched on was high, but the circulation pump flow rate ranged between 7 and 10, so instantaneous energy consumption was lower, and the operating time was shorter, reducing the cumulative energy. As with the heat pump, the circulation pump was efficiently operated in response to the partial load.

In [C-d], the FCU ran for a total of 275 min under rule-based control and 195 min for optimal control, and this was 162 and 106 min, respectively, for [A-a]. This was also believed to be because the system operated in response to partial loads, and the experimental results confirmed that the overall system operation time decreased when optimal control was employed.

For the FCU, energy consumption may increase because the system is continuously turned on and off according to optimal control. However, the circulation pump has a variable flow rate. Therefore, because the energy consumption for the circulation pump differs according to the flow rate, this energy consumption can be reduced even if the operation time is the same as the existing control. In addition, when the daily average outdoor temperature is similar, such as in the [C-d] and [A-a] sections, the operation time of the circulation pump and FCU was found to decrease.

The experimental results revealed that the most significant reduction in the energy consumption occurred in the heat pump within the system. Under rule-based control, even when the temperature range of the HST was outside the 8°C-12°C range, the system continued to operate. This means that, in rule-based control, if the HST temperature falls below the lower limit of 8 °C or rises above the upper limit of 12 °C, but 10 min have passed before the next control step, it continues to operate, resulting in continuous energy use. In addition, the system did not operate even if the upper limit of 12 °C was exceeded, so more energy could be used in the next control step. In contrast, under optimal control, the circulation pump flow rate was optimally controlled in the range of

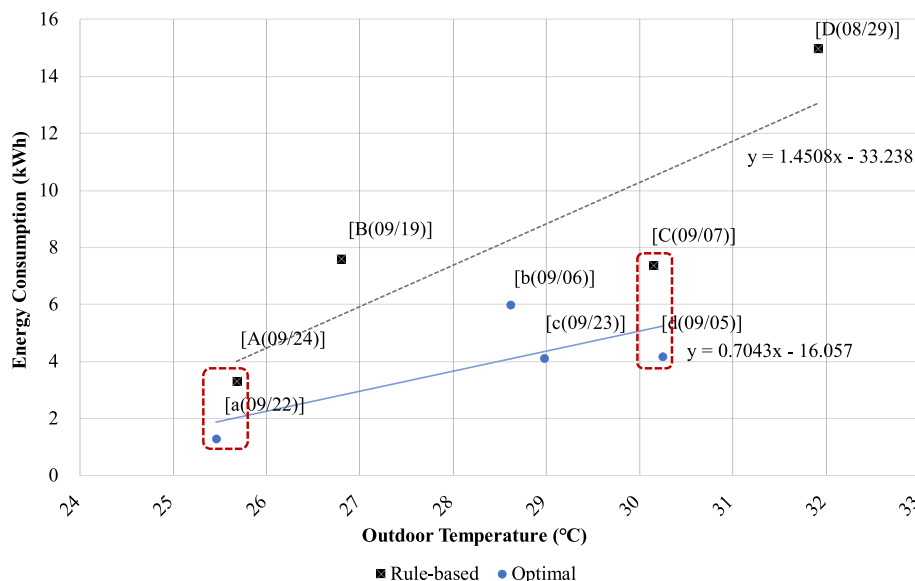


Fig. 8. Energy consumption of the hybrid heat pump system in relation to the daily average outdoor temperature.

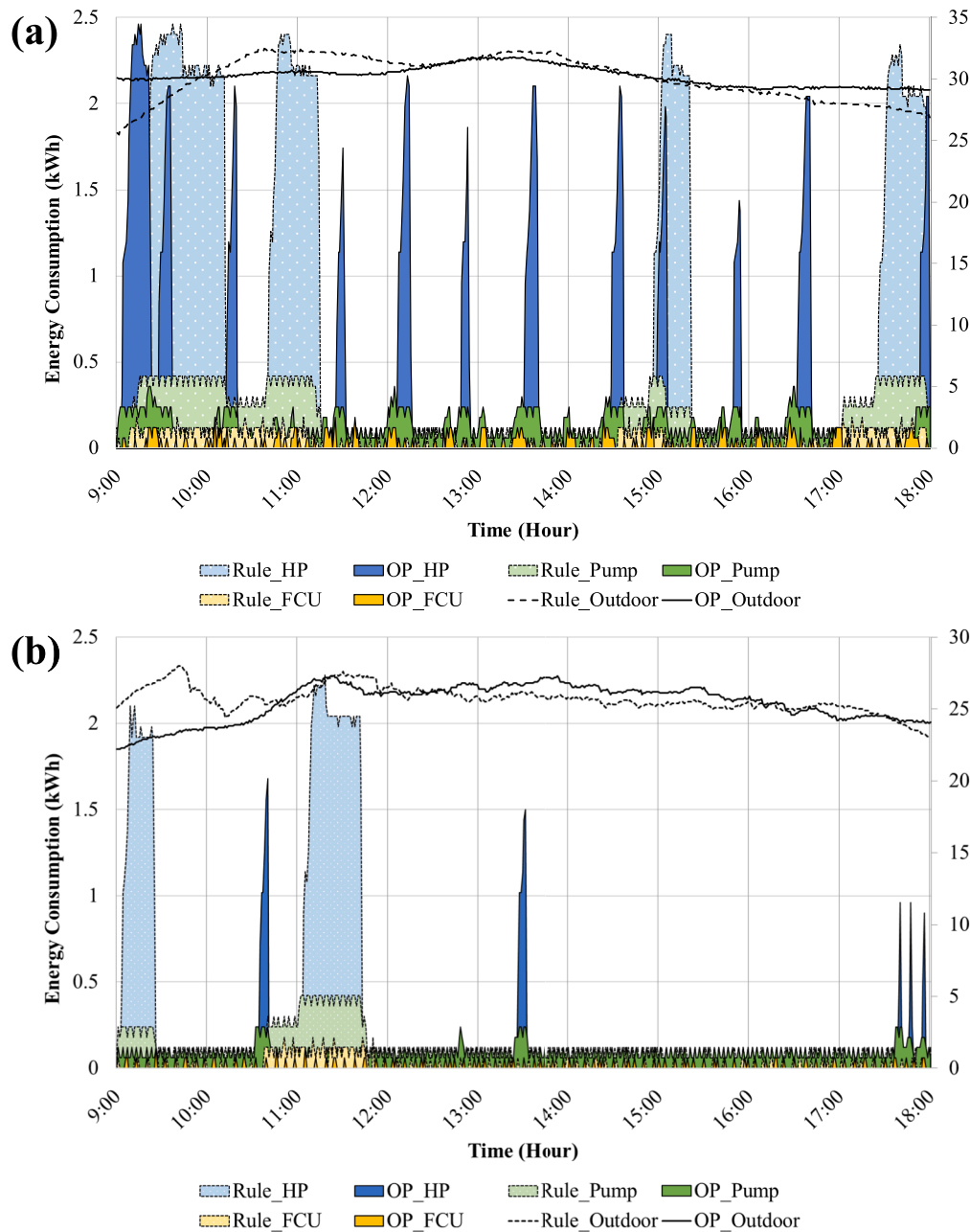


Fig. 9. Outdoor temperature and instantaneous power for the heat pump, circulation pump, and FCU for (a) C-d (09/07, 09/05), (b) A-a (09/24, 09/22).

7–10, allowing the heat pump to operate and stop in response to partial loads, preventing excessive use. This energy-saving behavior extended to indoor temperature control as well, with the circulation pump on the load side optimally controlled in the 0–10 range. During optimal control, although the number of individual system operation cycles for the heat pump and circulation pump increased in response to partial loads, the overall operating time decreased, reducing the overall system power consumption.

4. Conclusion

This study proposed an optimal control strategy for the integrated control of a hybrid heat pump system, with the goal of improving control performance and energy efficiency. For this purpose, an ANN-based predictive model was developed, which was then incorporated into an optimal control algorithm. An experiment was subsequently conducted

by embedding the optimal control algorithm in a hybrid heat pump system to test its control and energy performance. The following results and conclusions were drawn from the study:

- (1) To generate learning data for the predictive model, simulation modeling of the field system was conducted using TRNSYS 18. In this modeling, the circulation pump flow rate on the heat source side was set to levels 0 and 7 to 10, while the circulation pump on the load side was set to levels 0 and 10. Learning data was constructed by acquiring HST and room temperature data after 10 min following a change in the circulation pump flow rate. To meet the setpoints, an optimal control algorithm equipped with an on/off rule-based algorithm and the developed predictive model was constructed within the deadband range.
- (2) Two predictive models were developed: one that predicted the HST temperature and one that predicted the indoor temperature

10 min in the future. Both predictive models demonstrated excellent performance, surpassing the recommended ASHRAE standards (HST temperature prediction: $R^2 = 0.9988$, $CV(RMSE) = 1.06\%$, $NMBE = 0.16\%$, and $MAE = 0.09^\circ\text{C}$; indoor temperature prediction: $R^2 = 0.9893$, $CV(RMSE) = 1.66\%$, $NMBE = 0.16\%$, and $MAE = 0.15^\circ\text{C}$).

- (3) The HST temperature control performance of the optimal control algorithm was higher than the rule-based control method, with an improvement of 18.39 %, 3.10 %, and 1.31°C in terms of the $CV(RMSE)$, $NMBE$, and MAE , respectively. For indoor temperature, this improvement was 1.30 %, 0.42 %, and 0.29°C, respectively.
- (4) The energy savings resulting from the use of the optimal control algorithm were also assessed. The total system energy consumption was 17.57 kW, while that for the heat pump, circulation pump, and FCU was 14.07, 0.55, and 0.98 kW, respectively. This represented a reduction of 52.85 %, 61.39 %, and 6.56 % for total, heat pump, and circulation pump energy consumption, respectively, and an increase of 53.82 % for the FCU.
- (5) When the system energy consumption was compared with the average outdoor temperature, the energy consumption under optimal control was lower under similar outdoor conditions than under rule-based control, confirming its improved energy performance. In addition, when optimal control was employed, the number of system operations increased, but the overall operating time for the system decreased. In particular, the optimal control of the heat pump prevented overuse and resulted in the greatest reduction in energy consumption.

Collectively, these results demonstrate that the proposed ANN-based optimal control algorithm has the potential to generate significant energy savings in hybrid heat pump systems in a real environment. Based on these research results, future experiments are planned for the heating season, while the development of predictive models for energy consumption is necessary to select energy-efficient operating modes, particularly when using the heat produced by the PVT heat source during the heating period. In addition, there is a need to develop a bypass configuration that directly cools and heats the FCU using a heat pump, and a predictive model for the operating time to store heat and cool the HST in advance before operation. However, in this research, improvement in the performance of the prediction model through retraining was insufficient due to the short experiment schedule. Thus, the performance of the optimal control algorithm can be improved by conducting long-term experiments, building a corresponding database, and retraining the prediction model. Additionally, further research is needed to utilize PV power generation and PVT as a heat source. If these refinements are successful, it is believed that indoor comfort control and energy performance can be improved further with the use of the proposed intelligent optimal control algorithm.

CRediT authorship contribution statement

Yong Gi Jung: Data curation, Formal analysis, Methodology, Software, Supervision, Validation, Visualization, Writing – original draft, Writing – review & editing. **Kwang Ho Lee:** Data curation, Formal analysis, Validation, Visualization. **Bo Rang Park:** Data curation, Formal analysis, Software, Validation, Visualization. **Tae Won Kim:** Data curation, Formal analysis, Software, Validation, Visualization. **Jin Woo Moon:** Conceptualization, Formal analysis, Funding acquisition, Methodology, Project administration, Supervision, Writing – review & editing.

Declaration of competing interest

The authors declare that they have no known competing financial interests or personal relationships that could have appeared to influence

the work reported in this paper.

Data availability

Data will be made available on request.

Acknowledgments

This work was supported by the National Research Foundation of Korea(NRF) grant funded by the Korea government(MSIT)(No. RS-2023-00217322) and This research was supported by the Chung-Ang University Research Scholarship Grants in 2020 and This work was supported by the Korea Institute of Energy Technology Evaluation and Planning (KETEP) granted financial resource from the Ministry of Trade, Industry & Energy, Republic of Korea (No. 20213091010020).

References

- [1] CO2 emissions in 2022, 2022, International Energy Agency(IEA).
- [2] IPCC. (2014). AR5 Synthesis Report: Climate Change.
- [3] M. Franchini, P.M. Mannucci, Impact on human health of climate changes, *Eur. J. Intern. Med.* 26 (1) (2015) 1–5.
- [4] A. Haines, R.S. Lovats, D. Campbell-Lendrum, C. Corvalan, Climate change and human health: Impacts, vulnerability and public health. *Public Health*. Volume 120, Issue 7 (2006) 585–596.
- [5] L. Chen, G. Msigwa, M. Yang, A.I. Osman, S. Fawzy, D.W. Rooney, P.S. Yap, Strategies to achieve a carbon neutral society: a review, *Environ. Chem. Lett.* 20 (2022) 2277–2310.
- [6] Global Status Report for Buildings and Construction. (2021). Global Alliance for Buildings and Construction.
- [7] Energy Technology Perspective. (2017). IEA.
- [8] R.J. de Dear, T. Akimoto, E.A. Arens, G. Brager, C. Candido, K.W.D. Cheong, B. Li, N. Nishihara, S.C. Sekhar, S. Tanabe, J. Toftum, H. Zhang, Y. Zhu, Progress in thermal comfort research over the last twenty years, *Indoor Air* 23 (6) (2013) 442–461.
- [9] Y. Tong, T. Kozai, N. Nishioka, K. Ohyama, Greenhouse heating using heat pumps with a high coefficient of performance (COP), *Biosyst. Eng.* 106 (4) (2010) 405–411.
- [10] G. Gong, W. Zeng, L. Wang, C. Wu, A new heat recovery technique for air-conditioning/heat-pump system, *Appl. Therm. Eng.* 28 (17–18) (2008) 2360–2370.
- [11] B.R. Park, T.W. Kim, J.Y. Hyun, J.W. Moon, Climate-zone-dependent applicability of semi-transparent cadmium-telluride-type solar cells as a building material with display characteristics, *Energy. Buildings* 287 (2023) 112977.
- [12] R. Yokoyama, T. Shimizu, K. Ito, K. Takemura, Influence of ambient temperatures on performance of a CO2 heat pump water heating system, *Energy* 32 (4) (2007) 388–398.
- [13] E. Bisengimana, J. Zhou, M. Binama, K. Zhao, S. Abbas, Y. Yuan, The frosting and soil imbalance performance issues of building heat pumps: An overview, *Energy. Buildings* 273 (2022) 112387.
- [14] K.J. Chua, S.K. Chou, W.M. Yang, Advances in heat pump systems: a review, *Applied Energy* 87 (12) (2010) 3611–3624.
- [15] Element energy. (2017). Hybrid Heat Pumps, Final report. Department for Business, Energy & Industrial Strategy.
- [16] Y.J. Kim, E. Entchev, S.I. Na, E.C. Kang, Y.J. Baik, E.J. Lee, Investigation of system optimization and control logic on a solar geothermal hybrid heat pump system based on integral effect test data, *Energy* 129308 (2023).
- [17] Y.D. Jeong, M.G. Yu, Y.J. Nam, Feasibility Study of a Heating, Cooling and Domestic Hot Water System Combining a Photovoltaic-Thermal System and a Ground Source Heat Pump, *Energies* 10 (8) (2017) 1243.
- [18] W. Xu, C. Liu, A. Li, J. Li, B. Qiao, Feasibility and performance study on hybrid air source heat pump system for ultra-low energy building in severe cold region of China, *Renew. Energy* 146 (2020) 2124–2133.
- [19] T. You, B. Wang, W. Wu, W. Shi, X. Li, Performance analysis of hybrid ground-coupled heat pump system with multi-functions, *Energy. Conver. Manage.* 92 (2015) 47–59.
- [20] K. Klein, K. Huchtemann, D. Müller, Numerical study on hybrid heat pump systems in existing buildings, *Energy. Buildings* 69 (2014) 193–201.
- [21] S. Shang, X. Li, W. Wu, B. Wang, W. Shi, Energy-saving analysis of a hybrid power-driven heat pump system, *Appl. Therm. Eng.* 123 (2017) 1050–1059.
- [22] G. Bagarella, R. Lazzarin, M. Noro, Annual simulation, energy and economic analysis of hybrid heat pump systems for residential buildings, *Appl. Therm. Eng.* 99 (2016) 485–494.
- [23] Y.D. Jeong, Y.J. Nam, S.G. Yeo, Dynamic energy simulation for suitable capacity decision of GSHP-PVT hybrid system, *J. Architect. Inst. Korea Struct. Constr.* 33 (7) (2017) 53–61.
- [24] B.H. Sohn, Cooling performance analysis of ground-source heat pump (GSHP) system with hybrid ground heat exchanger (HGHE), *KSGHE* 14 (4) (2018) 43–52.
- [25] D. H. Park, T. W. Kim, J. Y. Byun, J. W. Moon. (2023). Development of Heat Storage Tank Temperature and System Energy Consumption Prediction Model for Photovoltaic Thermal and Air Source Hybrid Heat Pump. *KIEAE Journal*, 23(1), 31–36, 10.12813/kieae.2023.23.1.031.

- [26] E. Atam, D. Patteeuw, S.P. Antonov, L. Helsen, Optimal control approaches for analysis of energy use minimization of hybrid ground-coupled heat pump systems, *IEEE Trans. Control Syst. Technol.* 24 (2) (2016) 525–540.
- [27] W. Wei, C. Wu, L. Ni, W. Wang, Z. Han, W. Zou, Y. Yao. (2022). Performance optimization of space heating using variable water flow air source heat pumps as heating source: Adopting new control methods for water pumps.
- [28] A.K.S. Al-Sayyab, J. Navarro-Esbrí, A. Barragán-Cervera, S. Kim, A. Mota-Babiloni, Comprehensive experimental evaluation of R1234yf-based low GWP working fluids for refrigeration and heat pumps, *Energ. Convers. Manage.* 258 (2022) 115378.
- [29] S. Noye, R. M. Martinez, L. Carnieletto, M. D. Carli, A. C. Aguirre. (2022). A review of advanced ground source heat pump control: Artificial intelligence for autonomous and adaptive control. *Renewable and Sustainable Energy Reviews*, Volume 153, 111685. *Energy and Buildings*, Volume 255, 111654.
- [30] R. Tang, S. Wang, K. Shan, H. Cheung, Optimal control strategy of central air-conditioning systems of buildings at morning start period for enhanced energy efficiency and peak demand limiting, *Energy* 151 (2018) 771–781.
- [31] S.L. Wong, K.K.W. Wan, T.N.T. Lam, Artificial neural networks for energy analysis of office buildings with daylighting, *Appl. Energy* 87 (2010) 551–557.
- [32] J. Yang, H. Rivard, R. Zmeureanu, On-line building energy prediction using adaptive artificial neural networks, *Energ. Buildings* 37 (12) (2005) 1250–1259.
- [33] E. Wang, A.S. Fung, C. Qi, W.H. Leong, Performance prediction of a hybrid solar ground-source heat pump system, *Energ. Buildings* 47 (2012) 600–611.
- [34] W. Gang, J. Wang, Predictive ANN models of ground heat exchanger for the control of hybrid ground source heat pump systems, *Appl. Energy* 112 (2013) 1146–1153.
- [35] S. Sichelalu, H. Tazvinga, X. Xia, Optimal control of a fuel cell/wind/PV/grid hybrid system with thermal heat pump load, *Sol. Energy* 135 (2016) 59–69.
- [36] ISO 18523-1, (2016). Energy performance of buildings — Schedule and condition of building, zone and space usage for energy calculation —Part 1:Non-residential buildings.
- [37] F. Rosenblatt, The Perceptron — a perceiving and recognizing automaton, Cornell Aeronautical Laboratory, 1957. Report 85–460–1,.
- [38] J.W. Moon, Y.K. Yang, E.J. Choi, Y.J. Choi, K.H. Lee, Y.S. Kim, B.R. Park, Development of a control algorithm aiming at cost-effective operation of a VRF heating system, *Appl. Therm. Eng.* 149 (2019) 1522–1531.
- [39] Y.J. Choi, B.R. Park, J.Y. Hyun, J.W. Moon, Development of an adaptive artificial neural network model and optimal control algorithm for a data center cyber–physical system, *Build. Environ.* 210 (2022) 108704.
- [40] B.R. Park, Y.J. Choi, E.J. Choi, J.W. Moon, Adaptive control algorithm with a retraining technique to predict the optimal amount of chilled water in a data center cooling system, *Journal of Building Engineering* 50 (2022) 104167.
- [41] H.U. Cho, Y.J. Nam, E.J. Choi, Y.J. Choi, H.K. Kim, S.M. Bae, J.W. Moon, Comparative analysis of the optimized ANN, SVM, and tree ensemble models using Bayesian optimization for predicting GSHP COP, *Journal of Building Engineering* 44 (2021) 103411.